
Babeş-Bolyai University

Faculty of Physics



**Molecular Dynamics Investigations on Bio-macromolecular
Systems: from Mutant Huntingtin Model to D2-subunit
Dopamine Receptor and ssDNAs**

Summary of the doctoral thesis

Nastasia-Sanda Moldovean

Scientific Coordinator: Prof. dr. Vasile Chiş

2021

Cluj-Napoca

CONTENTS

1. Introduction	2
1.1 Scientific objectives	2
1.2 The structure of the doctoral thesis.....	3
1.3 Theoretical aspects.....	4
1.4 Huntington's disease and its genetic involvements.....	7
1.5 Structural features of mutant huntingtin structures	8
2. Results și discussion	10
2.1 Specific Key-Point Mutations Along the Helical Conformation of Huntingtin-Exon 1 Protein Might Have an Antagonistic Effect on the Toxic Helical Content's Formation	10
2.2 Decreased Interactions between Calmodulin and a Mutant Huntingtin Model Might Reduce the Cytotoxic Levels of Intracellular Ca ²⁺	14
2.3 All-Atom Molecular Dynamics Investigation on the Interactions between Dopamine D2 Receptor and Three 11 C-labeled Radiopharmaceutical Ligands	18
2.4 Biophysical Insights on the Interaction Mechanism between Multiple Single Stranded DNAs: A1/A2@GNR and miR21, anti-miR21, miR21-sp, random APT.....	22
3. Conclusions	27
Bibliography	29
List of publications and conferences	32

1.1 Scientific objectives

The doctoral thesis falls into the field of neuroscience and describes Huntington's genetic disorder that affects the central nervous system and causes progressive degeneration of neurons, involving autosomal dominant hereditary effects of motor and cognitive abilities. In this topic, the main purpose of the thesis is to characterize, from a biophysical point of view, the dynamics and structure of additional key-point mutations to the huntingtin mutant, with antagonistic effects on the formation of the toxic helical content within the DNA sequence. The obtained HTT model was characterized using molecular dynamics techniques. In short, the objectives of this study are:

- Development of a mutant structure with antagonistic effects on the formation of the toxic helical content within in the DNA sequence of huntingtin protein.
- Identification of the specific mutations and their characterization in terms of structural/dynamical changes of the entire huntingtin structure.
- Characterizing the dynamic behavior of the new mutant model and comparing it with other mutant structures and with the wild-type model, respectively, and determining the structural impact of the those particular mutations.
- Characterization of the interaction mechanisms between the proposed mutant (the 9P(EM) model) and another protein structure (calmodulin). The obtained results support the initial hypothesis of the present study, and confirms the deleterious behavior of the toxic helical content, while having a potential impact on the intracellular calcium levels by slowing down the cytotoxic cellular processes.
- Regarding the dopamine (DA) receptor, ligands labeled with ^{11}C isotope showed, according to the literature, higher binding affinities in the superior part of the receptor. Also, the interaction energies highlighted two potential candidates for diagnostic techniques: ^{11}C -RACL ligand docked at the top part of the receptor (in good agreement with the literature) and ^{11}C -SCH docked at the bottom part of the receptor; the latter ligand represents a new potential candidate for the dopamines' quantification at the cerebral level.
- The binary and ternary systems composed of single-stranded DNA chains showed strong interactions, consistent with experimental data obtained in the same study, based on similar

structural behaviors and the identification of neighboring nucleotides according to the chemical complementary rules.

1.2 The structure of the doctoral thesis

The introductory chapter describes the theoretical approaches of molecular dynamics techniques used for structural and dynamical investigations of complex bio-macromolecular systems and establishes the main objectives of the thesis. Chapter 2 highlights the essential biological sections of the human brain and other physiological components directly involved in synaptic transmissions. Huntington's disease is also pathologically characterized, along with its genetic implications and structural changes that may occur at the polyglutamine tract's level and at the flanking regions' domains.

Chapter 3 presents in detail the integration of all methodological steps taken into account for the generation of the MD trajectories.

The presented results in Chapter 4 are divided into five parts. The first three parts are based on published research articles on Huntington's disease. The first article summarizes and analyzes the literature focused on theoretical investigations involving the use of molecular dynamics methods, compared with experimental studies, on physiological and mutant huntingtin protein structures (*Molecular Dynamics simulations applied to structural and dynamic transitions of the HTT protein: A review*). The second article (*Specific key-point mutations along the helical conformation of Huntingtin-Exon 1 protein might have an antagonistic effect on the toxic helical content's formation*) describes our proposed 9P(EM) model. This model with additional mutation points suggests promising structural/dynamical behavior, providing an antagonistic effect to the mutant huntingtin protein (insoluble in organic solvents and extremely toxic). The third article is based on the study of the interaction mechanism between the 9P(EM) model and another structure of interest (a Ca^{2+} binding protein), demonstrated in the experimental literature to colocalize with huntingtin structures in the brain (*Decreased Interactions between Calmodulin and a Mutant Huntingtin Model Might Reduce the Cytotoxic Level of Intracellular Ca^{2+} : A Molecular Dynamics Study*).

The last two parts correspond to molecular recognition and targeted intermolecular interactions that, for future purposes, provide important aspects for the experimental implementation of our mutant

huntingtin model. Thus, the fourth article characterizes the geometry and the binding strengths of three [^{11}C]-labeled radiopharmaceuticals compounds widely used for dopamine receptor's quantification at the cerebral level.

Ultimately, in the last research paper, specific interactions between multiple single stranded DNAs attached onto the gold surface were studied, following the assumption that the most stable and complementary-based interactions should provide insightful details for novel molecular approaches to therapeutic developments.

Considering the previously mentioned aspects, the final conclusions and the experimental perspectives are presented in the last chapter of this thesis.

1.3 Theoretical aspects

The theoretical biochemical approaches have been widely used over the past decades with an initial focus on force-field based calculations for biomolecular systems' characterization from structural and dynamical point of views. The combined quantum mechanics/molecular mechanics (QM/MM) with classical molecular dynamics (MD) techniques enable an accurate description on the biophysical properties of the intermolecular and intramolecular interactions [1]. These approaches vary depending on the size and complexity of the systems of interest, covering *ab initio* quantum methods with functionals based on the electronic densities, and atomistic methods often used to characterize larger systems, such as macro-biomolecular ones [1].

The *model notion* (using molecular modeling techniques) in the theoretical concept is related to a simplified or idealized description of a group of atoms, with their related potentials, meant to imitate the real behavior of molecules and/or molecular systems. Most systems studied by molecular modeling cannot be characterized by quantum approaches due to the large number of constituent particles and due to the inclusion of electrons in the model of interest. On the other hand, the force field method (or mechanical modeling) neglects the movement of electrons and treats the energy of the system as a function of nuclear positions, allowing the study/prediction of the systems with a large number of atoms [1].

The introductory chapter presents the essential theoretical concepts for describing the dynamic evolution of individual protein structures, as well as protein-protein and protein-ligand

interaction systems. Theoretical biophysical studies, at the molecular level, can be performed taking into account atomic movements, the key factor in determining the properties of living systems, with a further description of the correlation between structure and function [2]. This relationship also plays a key role in the dynamics of complex systems, where any structural change influences the dynamic characteristics, respectively the functionality, of biomolecules.

Molecular self-assembly (the polypeptide chain packing in space) is regulated by hydrogen bond networks (between peptide groups in the same chain or adjacent chains) which give the structure of interest a certain shape. These shapes, also called secondary structures, can be helical (or spiral), can have flat conformations like free chains (also known as *loops*), or can be arranged in layers (*β -sheets*) [2]. From a geometrical point of view, the number of these possible configurations is infinitely large. In reality, however, the protein configurations are determined by the sequence of the constituent amino acids, thus fluctuating around an average configuration corresponding to its minimum free energy. Given the structural complexity of protein systems, their tertiary structure can only be determined by using X-ray diffraction experiments [2].

Intrinsic molecular assemblies are based on intramolecular interactions described by the bonds formed between the atoms of polypeptide chains. Also, the reproduction of the structural properties for complex systems can be achieved with the help of force fields [3]. The transferability of structural units, called "building-blocks", aims to parameterize a group of atoms (for example, a simple hydrocarbon such as alkane) that can then be applied to any other group of atoms corresponding to the group originally declared. In other words, in the force fields, the structural units must be parameterized only once. Thus, another important aspect is the declaration of each atom type. For a more accurate description of a system, the force field parameters must differentiate atoms (of the same kind), while varying degrees of substitution or hybridization states (differentiation between a carbon atom of an alkane with sp^3 hybridization type and a carbon atom corresponding to a benzene nucleus with sp^2 hybridization type) [3].

All force fields are based on the following components that describe the intra- and inter-molecular interactions in a given system [4]:

$$V(r_1, r_2, \dots, r_N) = \sum_{bonds} \frac{1}{4} K_b (b^2 - b_0^2)^2 + \sum_{angles} \frac{1}{2} K_\theta (\cos\theta - \cos\theta_0)^2 + \sum_{impropers} \frac{1}{2} K_\xi (\xi - \xi_0)^2 + \sum_{dihedrals} K_\phi [1 + \cos(\delta) \cos(m\phi)]^2 + \sum_{pairs} \left(\frac{C12_{ij}}{r_{ij}^{12}} - \frac{C6_{ij}}{r_{ij}^6} \right) + \sum_{pairs} \frac{q_i q_j}{4\pi\epsilon_0\epsilon_1} \frac{1}{r_{ij}} \quad (1.1)$$

The declared parameters within a force field, such as GROMOS, OPLS, CHARMM and AMBER, are chosen so as to reproduce the data obtained by experimental methods. On the other hand, the diversity of small organic molecules makes impossible the use of parameters already obtained in the case of similar molecules, and requires an individual parametrization (atom by atom) of each compound [4].

1.4 Huntington's Disease and its genetic involvements

Huntington's disease is an autosomal dominant neurodegenerative disorder, caused by a genetic defect located in the Huntingtin gene on chromosome 4, causing the slow and progressive death of nerve cells in the brain. The genetic modification consists in a quantitative expansion of the trinucleotide groups CAG (cytosine-adenine-guanine) at the level of the first constituent exon of the HTT sequence. The trinucleotide group CAG encodes glutamine aminoacid from the huntingtin protein. The polymorphic repetitive sequence contains, variably in healthy members of the population, 11-34 CAG units. On the other hand, during cell division, the number of repeats of these nucleotides may increase (expansion), and an increase of over 35 in the number of CAG units determines the disease's threshold. The mechanisms of intra-molecular interaction characteristic of HTT mutant self-assembly processes remain unknown, but the polymerization of CAG tracts requires an aggregation rate directly proportional to the extension of the polyglutamine tract's length (with the number of polymerized CAG groups). In this perspective, the expansion of polyglutamines induces a local phenotype with toxic functions, while low concentrations of physiological HTT proteins could also induce specific mutant aggregates as a side or incidental effect of the disease [5].

Neurons (*Figure 1, left*) represent the morphofunctional units of the nervous system and are responsible for releasing chemical signals, supporting the neural network and transmitting impulses to other target cells. The electrochemical signal transmissions are generated by synaptic junctions (*Figure 1, right*). Electrical synapses are responsible for electrical connections between two or more neurons, while chemical synapses involve synaptic transmission through specific chemicals (neurotransmitters) embedded in synaptic vesicles located on both terminals of the synaptic junction [6].

In the context of Huntington's disease, the excessive polymerizations previously discussed, at the level of the first exon, facilitate the accumulation of mutant structures, avidly and insoluble in organic solvents, in the pre-synaptic neuronal component. These accumulations, known as cerebral inclusions, are mainly formed in the neuronal nucleus, subsequently inducing cell apoptosis (death). Destroyed neural networks are characterized by motor disorders (of movements), typical

uncontrolled spasmodic movements, progressive loss of mental abilities and cognitive functions, behavioral changes, psychotic manifestations and epileptiform seizures [5].

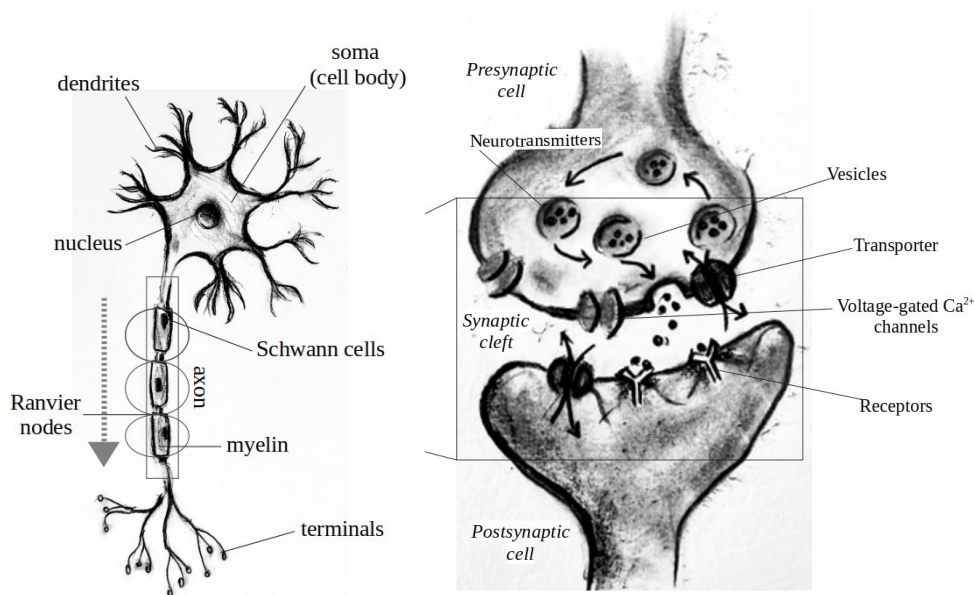


Figure 1. Schematic representation of a neuron (left) and the synaptic transmission components(right).

1.5 Structural features of mutant huntingtin structures

The best characterized part of the entire wt-sheet conformations.HTT sequence is the exon 1 (Ex.1) (*Figure 2*) where the HTT mutation takes place, with an N-terminal domain consisting of 17 amino acids, followed by the wild-type or mutant polyglutamine (polyQ) stretch and ends with a proline-rich (polyP) domain (PRD) which is considered to act as an active protein-interacting domain [7, 8]. Most of the published review articles [9-13] focused on elucidating the HTT's biological mechanisms. However, in this sense it is crucial to understand the mutants structural transitions from their monomeric states into aggregated fibrils, with a primarily presumption that simple polyQ monomers might be actually intrinsically toxic, therefore an optimal way to address HTT protein's structural stability with its aggregation behavior is to assess those conformational changes on different types of models. Hence, all-atom MD productions of the entire Ex.1-HTT protein were made using different polyQ lengths.

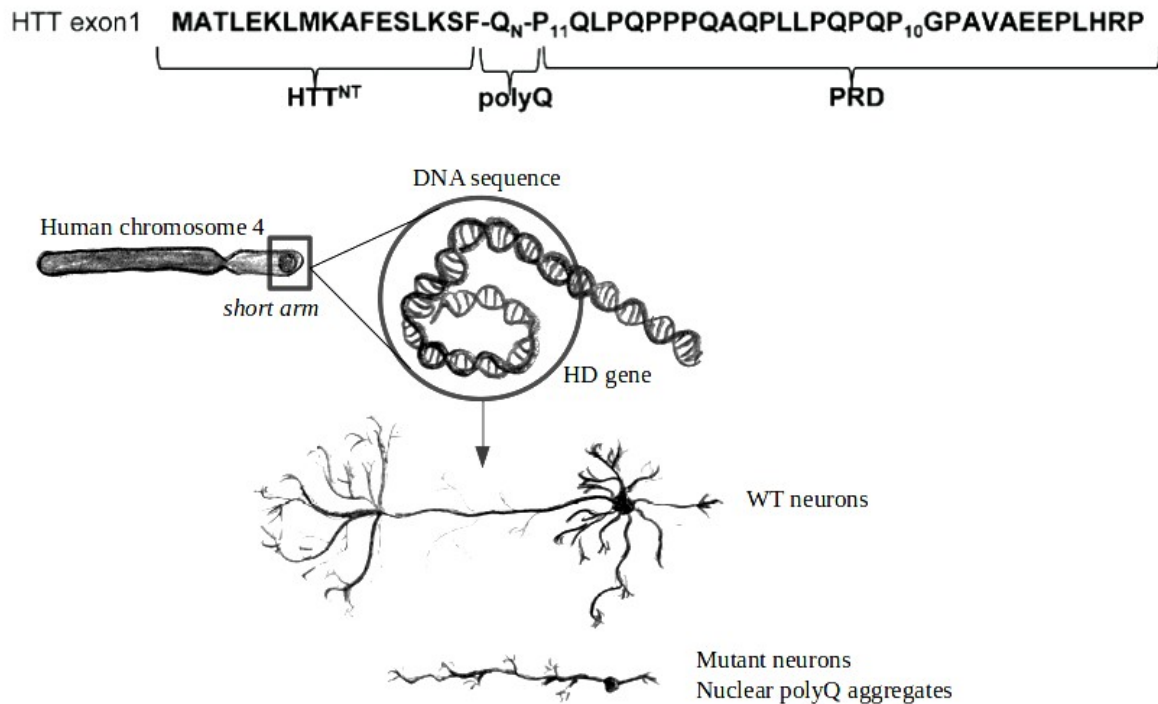


Figure 2. Wild-sheet conformations.type HTT-Exon1 sequence (top) with its localization at the chromosome's level (middle) and the neuronal morphology upon HD onset (bottom).

In many cases, the presence of polyQ tracts longer than 36–40 glutamine (Qs) has been associated with drastic structural transitions from random loops to β -sheet conformations [14 - 16]. Consequently, it is considered that for a higher number of Qs, the elasticity of HTT proteins increases [17-19]. On the other hand, studies have also shown that shorter polyQ fragments tend to have same structural behavior and adopt similar configurations (post-aggregation) to those characteristic of a larger number of Q residues [20].

Another characteristic model of the insoluble toxic components generated as a result of the excessive polymerization of glutamines, is the β/α -helical configuration model [21]. Considering that the main contradiction found in the literature is related to the secondary structure, some articles reported that the monomeric state of HTT-Ex.1 conformations is dominated by α -helices [20-24], while other studies suggested that the rate of formation of β -sheet configurations increases with increasing number of Qs [25, 26].

2.1 Specific Key-Point Mutations Along the Helical Conformation of Huntingtin-Exon 1 Protein Might Have an Antagonistic Effect on the Toxic Helical Content's Formation

The first study aims to characterize the dynamic behavior and structural changes related to the toxic helical structure of the mutant huntingtin protein, where additional mutation points from glutamine (GLN) amino acid to proline amino acid (PRO) located randomly along the helix were implemented (R models), at the helical edges (E models), respectively at the edges and in the middle of the helix (EM models), according to *Figure 1*.

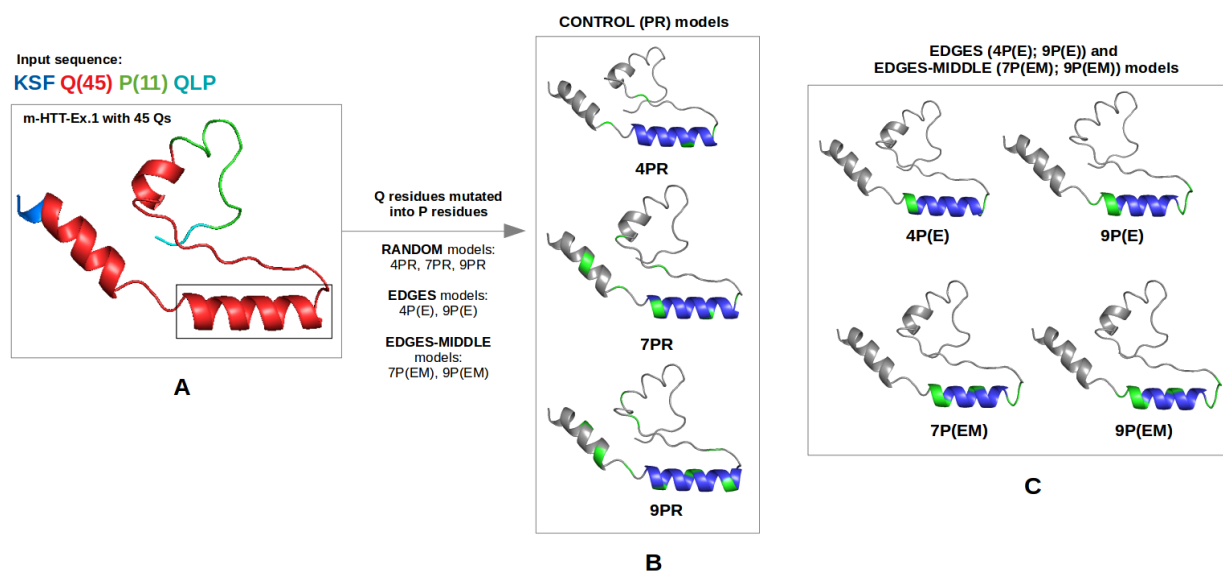


Figure 1. Schematic representation of the additional mutations (in green) applied along the HTT-Exon1 sequence.

The results show an increased level of compactness for models with a higher number of mutations (models 7P and 9P) with specific mutations at the edges, respectively at the edges and in the middle of the helical content (*Figure 2*). Moreover, the distances between the alpha carbon atoms (chiral atoms) at the edges of the helix decreased for the 7P and 9P models, compared to the 4P models. Also, from a dynamical point of view, the atomic fluctuations (RMSF profiles) showed maximum (average) values for the 9P models with point mutations at the edges and in the middle of the helix. In addition, secondary structure analysis suggests structural transitions from insoluble (or hardly soluble) α -helical structural components into soluble loops and *random coils* for the 7P and

9P models, especially for models in which point mutations have been considered at the edges and in the middle of the helical content.

The random models (4PR, 7PR and 9PR) suggest similar structural behavior, regardless of the number of mutations initially considered. For the gyration profiles, the average values for 4PR and 9PR were 0.79 nm and 0.78 nm, while the average Rg value for the 7PR model was 0.77 nm. Therefore, the relevance of the key-point mutated residues (from GLN into PRO amino acid) in random models is insignificant.

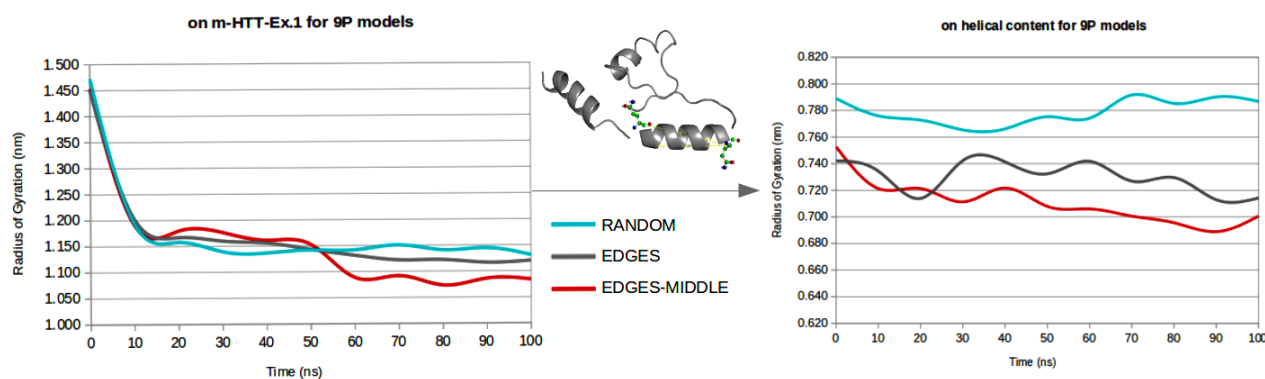


Figure 2. Radius of gyration plots for the full input sequence (left) and the helical content of interest (right) of the nine PRO mutant models.

Regarding the specific mutations for models E and EM, the Rg values showed significant variations directly correlated with drastic structural changes. Here the gyration measurements showed decreased values for higher number of P mutated residues situated at the edges of the helix (0.74 nm for 4P model and 0.73 nm for 9P model) and even lower values of 0.71 nm for the 9P models with point mutations at the edges and in the middle of the helix. Moreover, these resulted unfolded states at the level of the helix are strongly correlated with large conformational changes and with reduced motifs for helical secondary structure's formation.

For the 4P(E) model, the average RMSF value (*Figure 3*) was 0.18 nm, in comparison to the RMSF value of 0.25 nm for model 9P(EM). These increased fluctuations in the RMSF profile of the 9P(EM) belong to the previously discussed conformational transitions. Moreover, according to the residual fluctuations, the RMSF values were higher for the indexed residues 24-30, indicating partial disruptions of the helical content but from a certain direction (from the PRD terminus to the N17 terminus).

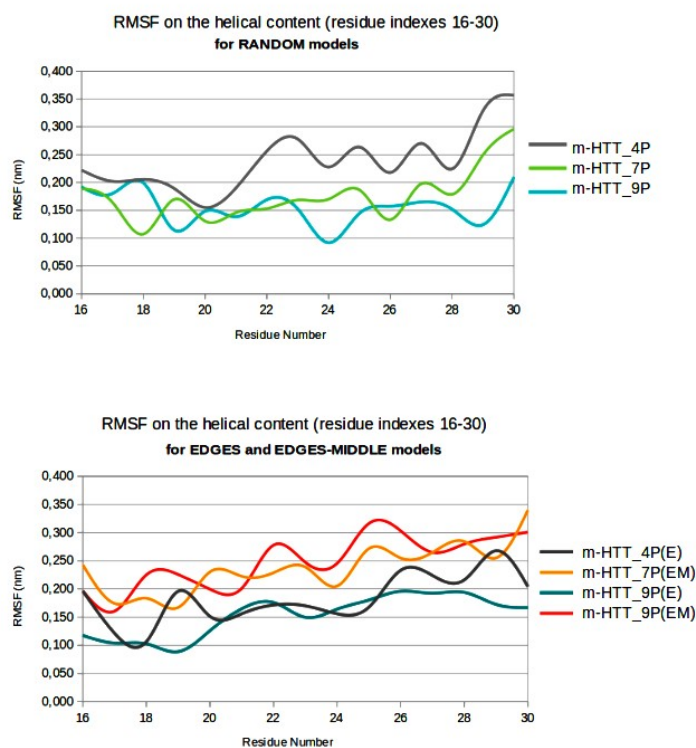


Figure 3. RMSF per residues (for residue numbers 16–30) for random models (top) and for edges and edges-middle models (bottom).

The largest distance of 2.16 nm was noted for the 9P random model, while the smallest distance of 1.66 nm was seen for the same model but with point mutations on the edges and in the middle of the helix (for the 9P(EM) mutant model). As initially hypothesized, as the number of mutations increases, the spot of mutation becomes crucial. From the plotted results, we can consider that starting with a higher number of mutations (>9P mutation points), the occupied mutation spots that promote the helical disruptions are on the edges and in the middle of the helix.

For the mutation points related to the 4P model, the largest atomic fluctuations were observed at the level of the first five terminal residues (KSFQQ) characterized by *loop* configurations. Thus, the 4P (R) and 4P (E) models, although they appear to be extremely flexible, they involve little to no conformational changes, without having a direct impact on the toxic glutamine chain.

In general, the highest local fluctuations involving structural drastic changes at the level of the helix (Figure 4), were observed for the KSFQ residues (atomic indices 1-5), QQ (indices 14-15)

and QPP (atomic indices 29- 31). The dynamics behind these residual groups indicate that models with mutations considered at the edges of the helix are more likely to pull the entire structure from both ends, imposing minimal (elongation) structural changes on the central portion (indexed atoms 14-15). On the other hand, for the 9P(EM) model the increased RMSF values were also correlated to the PRO residues considered in the middle of the polyQ tract.

Moreover, for the same model, maximum fluctuation rates were also obtained for the GLN and PRO residues located at the edges of the helix. Although the N17-terminal domain's fluctuations are independent from the polyQ helical content, this model shows significant and correlated structural changes for the 29-31 indexed residues, related to the structural components located at the right helical end. These findings could indicate that the helical disruption is predominantly oriented towards the conformations of the external components (N17 and PRD), and that these increased fluctuations at the helical level may also affect the stability of the adjacent domains (the flanking regions). In agreement with the results discussed above, for the proposed 9P(EM) model as a mutational threshold, the mean axis length corresponding to the toxic helix was 1.23 nm, with a maximum elongation value of 1.36 nm.

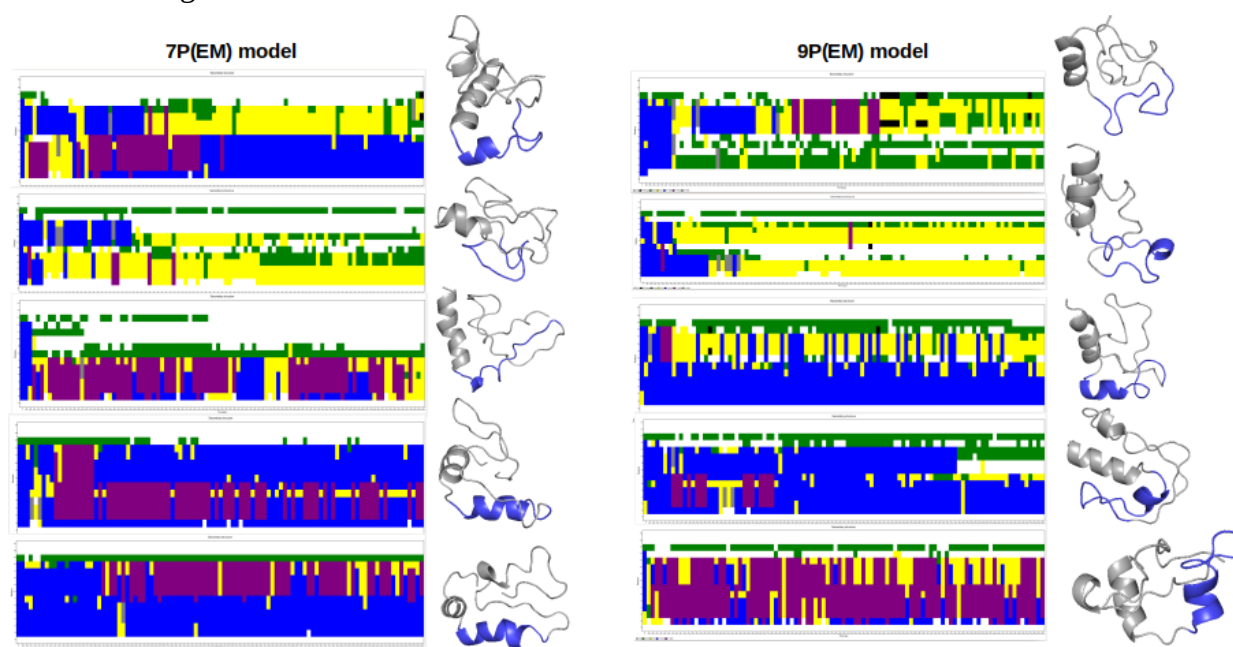


Figure 4. Secondary structure of edges-middle models and the selected corresponding structures (per run) on the right, with the resulting helical content (in blue).

2.2 Decreased Interactions between Calmodulin and a Mutant Huntingtin Model Might Reduce the Cytotoxic Levels of Intracellular Ca²⁺

The experimental studies have shown that huntingtin mutant proteins and Ca²⁺-binding structures co-localize in the cerebral cortex, with significant effects on the intracellular calcium levels, by altering specific calcium-mediated neuronal signals. Due to the fact that mutant HTT proteins have an increased affinity for Ca²⁺ binding molecules, interactions between them can lead to further stabilization of mutant HTT aggregates. In this context, the following study focuses on the description of the interaction mechanisms between calmodulin (CaM) and two HTT mutants, including the previously hypothesized and debated 9P(EM) mutant model.

According to the figure illustrated below, the CaM interacting complexes, obtained by molecular docking techniques, contain a physiological or wild-type huntingtin structure (with 9 glutamine residues), a mutant with 45 glutamine residues (45Qs-HTT model) and the 9P(EM) model with additional mutation points (from GLN to PRO) at the edges and in the middle of the helix.

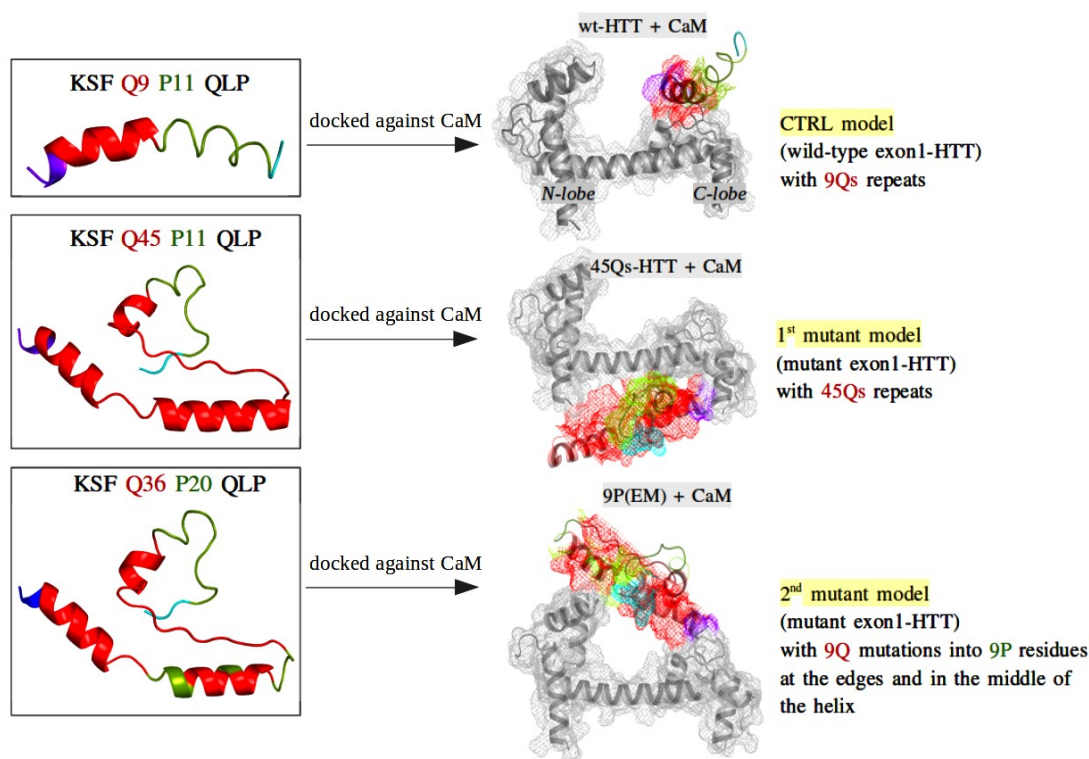


Figure 5. Input WT and mutant HTT models (left) used for further HTT-CaM (right) MD productions for 100 ns.

For the wt-HTT model (*Figure 6, top-left*) the docked complex presented a total binding free energy of -32.90 kcal/mol from which the polar components (ΔE_{ele} and ΔG_{polar}) make a positive contribution of 0.77 kcal/mol. The van der Waals interaction energy for this complex was -28.93 kcal/mol and was noted as the lowest absolute value among all complexes. The non-polar component for the same docked complex was -4.73 kcal/mol, being the lowest absolute value obtained for the hydrophobic contributions. The lowest binding pattern with a total binding free energy value of -23.38 kcal/mol was obtained for CaM-45Qs HTT docked complex (*Figure 6, top-right*), with similar electrostatic energy value of -962.41 kcal/mol as for CaM-wt-HTT complex. The polar contributions for this complex presented the highest positive value of 48.94 kcal/mol (with $\Delta G_{\text{polar}} = 1011.35$ kcal/mol).

For the CaM-9P(EM) complex (*Figure 6, bottom*) the total binding free energy was -38.31 kcal/mol. The overall contribution values for each energy component were in between the two other docked complexes (CaM with wt-HTT and 45Qs-HTT models). The obtained non-polar solvation free energy ($\Delta G_{\text{nonpolar}}$) was -6.81 kcal/mol, while for the polar contributions the ΔG_{polar} and the electrostatic interaction values were 835.31 kcal/mol and -825.03 kcal/mol, respectively. In the same manner as for the 45Qs-HTT model, the van der Waals energy value for the 9P(EM)-CaM was -41.78 kcal/mol, indicating that the molecular shape of these interacting partners present a great influence on the molecular recognition processes of the CaM protein.

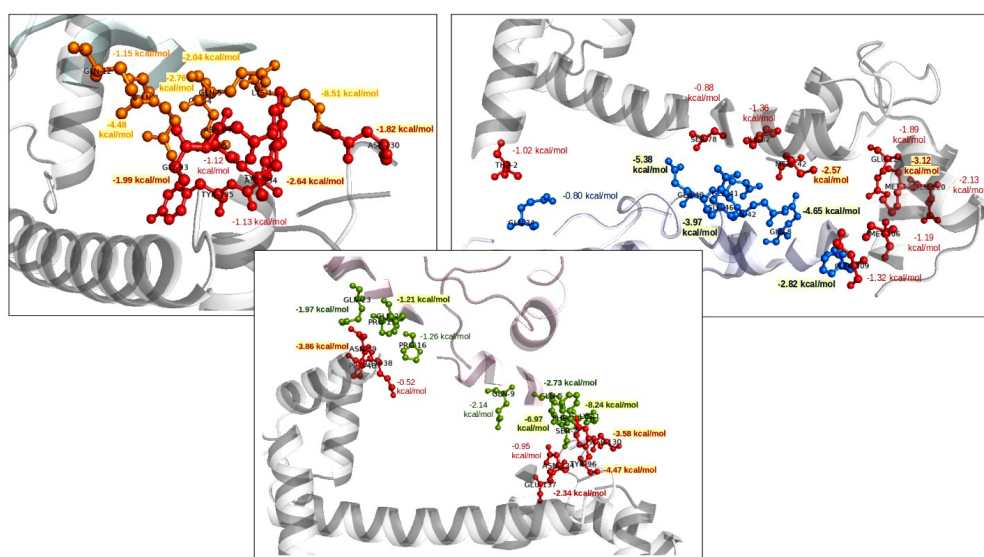


Figure 6. Per-residue contributions for CaM and wt-HTT (top, left), 45Qs-HTT (top, right), 9P(EM) (bottom) docked complexes.

The lowest RMSD values were obtained for the CaM-9P(EM) interaction complex, where the maximum average values ranged between 0.71-0.76 nm. Increased variations in RMSD values for CaM in interaction with the wt-HTT model are most likely caused by the increased flexibility rates due to *loop* configurations, thus promoting an increase in the number of degrees of freedom for CaM structure.

The lowest gyration profile, meaning the highest compactness levels, was observed for CaM protein in its interactions with the 9P(EM) model (*Figure 7, top-right*), where the minimum distance value between the calmodulin's lobes was in fact the maximum average value of 0.77 nm. An intermediate (average) distance value of 0.57 nm between the N lobe and C lobe was obtained for the CaM structure in its interaction with the 45Qs-HTT mutant model. For the wt-HTT model, due to the short glutamine sequence and, consequently, to a smaller number of helical components, the average Rg value was 1.22 nm and remained constant throughout the trajectories showing the smallest variations among all HTT models. In addition, a maximum average RMSF value of 0.34 nm was obtained for the wt-HTT model, while the 45Qs and 9P(EM) mutants showed similar dynamic behavior.

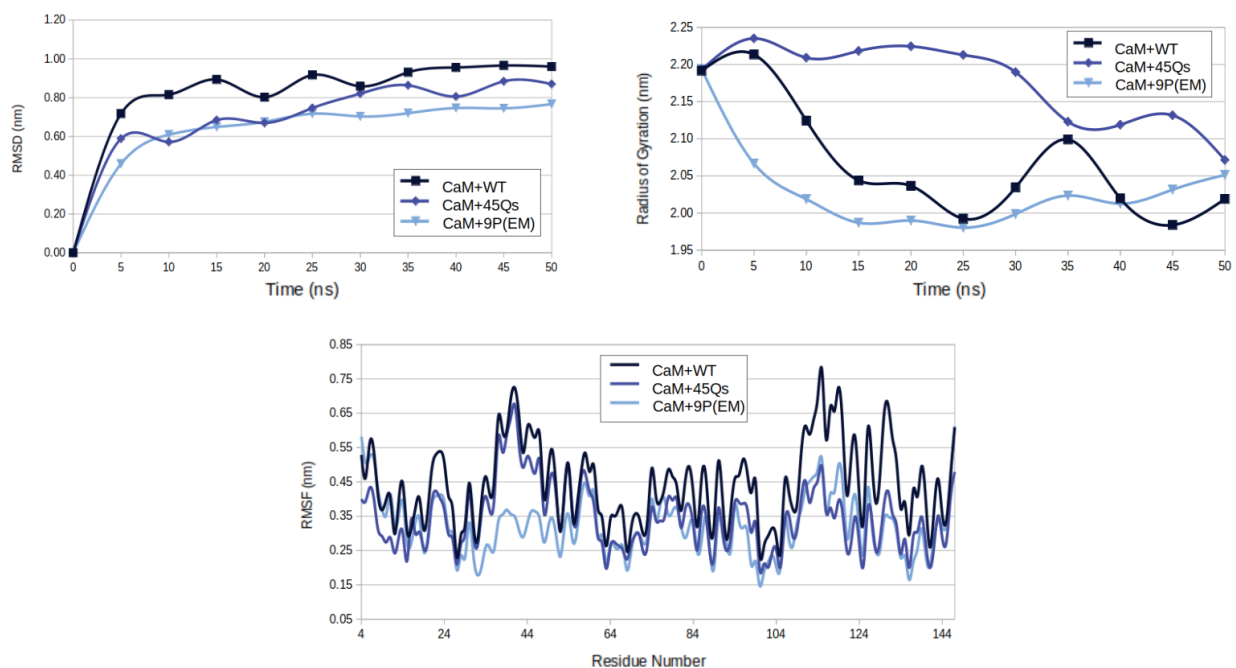


Figure 7. RMSD (top, left), radius of gyration (top, right) and RMSF (bottom) profiles for CaM protein in its interaction with HTT models.

The wt-HTT model indicates a general preservation of its helical contents. On the other hand, the 45Qs-HTT structure has a minimum average distance between the ends of the helix of 1.79 nm, while for the 9P (EM) mutant model the minimum average distance was 1.42 nm. Both mutants had an initial helical distance of approximately 2.20 nm, and the 45Qs-HTT model showed a significant decrease to 1.66 nm after 30 ns of MD production. Moreover, the 9P(EM) model showed, after only 20 ns, a minimum distance between the edges of the helical content of 1.27 nm.

For the 9P (EM) mutant model (*Figure 8*) the number of helical configurations significantly decreases [27], these changes promoting slightly lower SASA values compared to the 45Q-HTT mutant and consequently higher RMSF values, eventually being correlated with the obtained (low) interaction energies between CaM and 9P(EM) model.

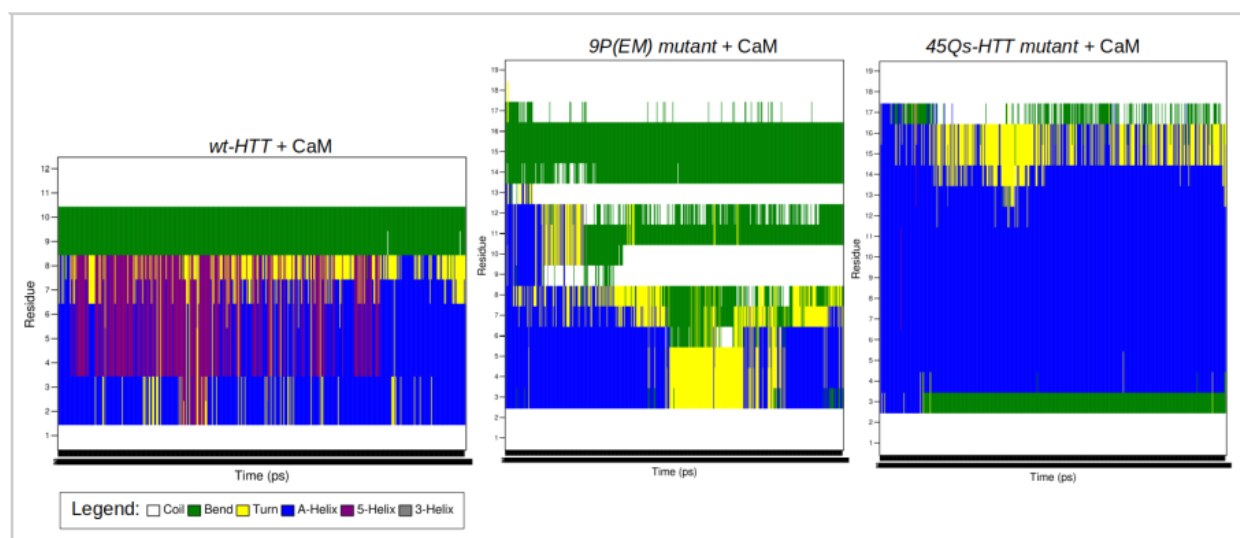


Figure 8. The secondary structure analysis for HTT models in interaction with CaM.

This study confirms that the total interaction energy between the CaM and wt-HTT model is -130.11 kcal/mol and, according to our hypothesis, a much higher interaction energy value of -313.87 kcal/mol was obtained for the interactions between CaM and the 45Qs-HTT structure. Moreover, an intermediate (average) interaction energy value of -238.95 kcal/mol was observed for the 9P(EM) mutant model [28].

2.3 All-Atom Molecular Dynamics Investigation on the Interactions between Dopamine D2 Receptor and Three ¹¹C-labeled Radiopharmaceutical Ligands

A direct correlation between huntingtin mutants and dopamine (DA) neurotransmitters is that they can trigger uncoordinated movements and other pathological profiles (like severe cognitive symptoms) in subjects with HD or with alterations of DA at the striatum level. There are evidence that suggest an involvement of nigrostriatal DA in HD implying increased levels of DA (in HD postmortem brains) and that some DA receptor agonists can be used for therapeutic purposes. In contradiction, there are also studies that showed reduced levels of caudate DA in late stages (postmortem) HD patients. As an extension, the DA uptake mechanism in HD and its selective affinity are of an essential matter before pursuing with the description of any other specific dopaminergic signalling, therefore the following research study aims to characterize the D2-subunit of DA receptor in its interaction with three [¹¹C]-labeled ligands, extensively used nowadays for D2 dopamine receptor's quantification.

The results of this study, following the imposed molecular docking techniques, show that the hydrophilic and hydrophobic profiles (*Figure 9*) have lower values for the ligands docked at the top part of the receptor, implying that the ligands remained inside their docked positions of D2DR. The highest average SASA value of 5.63 nm² was observed for the FLB ligand docked at the bottom part of the receptor. The aliphatic chain of the FLB ligand shows large dynamic fluctuations, due to the secondary structure components (*loop* configurations) of D2DR in its lower part. The maximum measured SASA value noted for the same ligand was 6.32 nm.

Moreover, for both D2DR docked positions, the FLB ligand showed the highest rotational angle value of 0.41 nm. The lowest average Rg value of 0.34 nm was observed for the SCH ligand docked at both D2DR's interaction ends, although the largest changes in ligand compactness profiles during the simulations were described for the RACL ligand docked at both ends of the receptor.

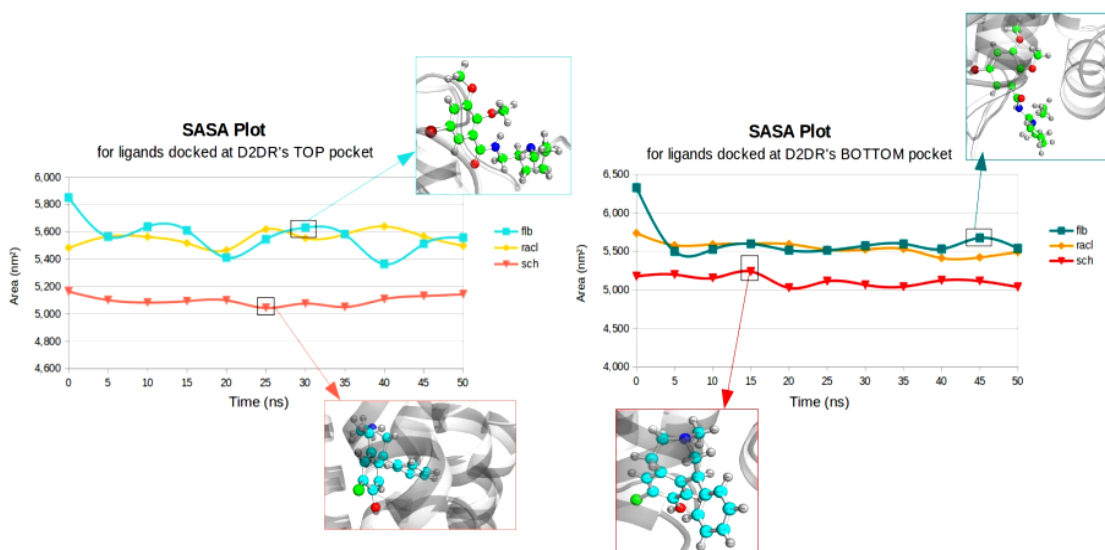


Figure 9. SASA profiles for ligands docked at D2DR's top (left) and bottom (right) position.

The lowest atomic fluctuations were obtained for the SCH ligand (Figure 10), these results being consistent with lower mean rotational values of 0.34 nm and high hydrophobic profiles described by the lowest SASA values for both D2DR's docked positions. Similarly, a strong correlation was observed between the increased degree of flexibility of the RACL ligand and its gyration behavior, when its average compactness values are taken into account.

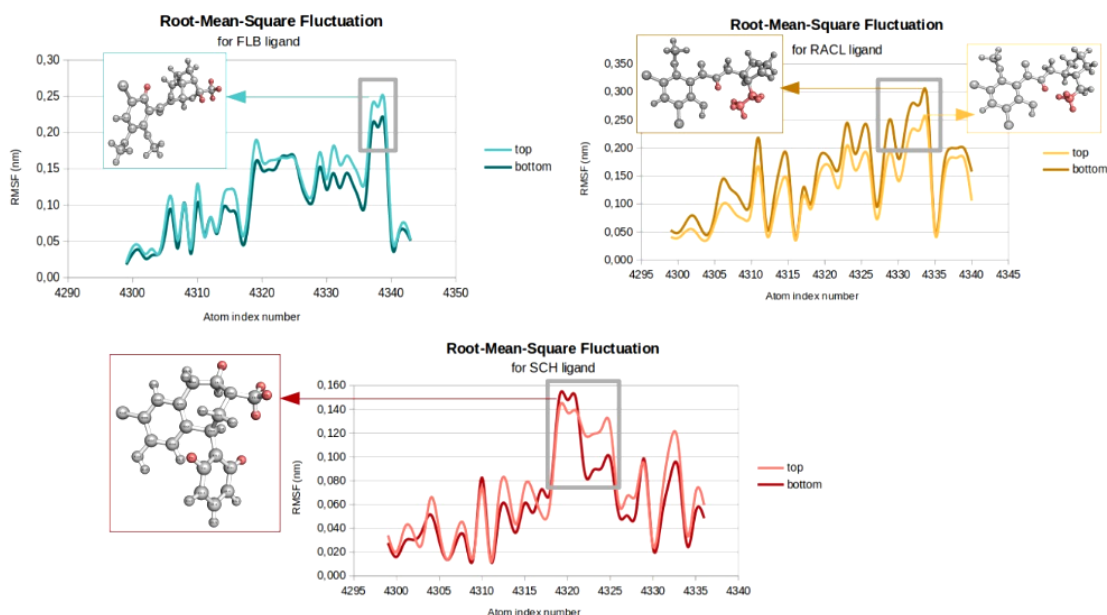


Figure 10. RMSF plots of D2DR's docked ligands.

Moreover, for ligands docked at the superior part of D2DR, the rotary bonds illustrated in *Figure 11* promote drastic conformational changes of FLB and RACL compounds, therefore promoting great translational and torsional motions. The ethylamine component (CH₃-CH₂-N-) has, in most cases, a rotary motion type.

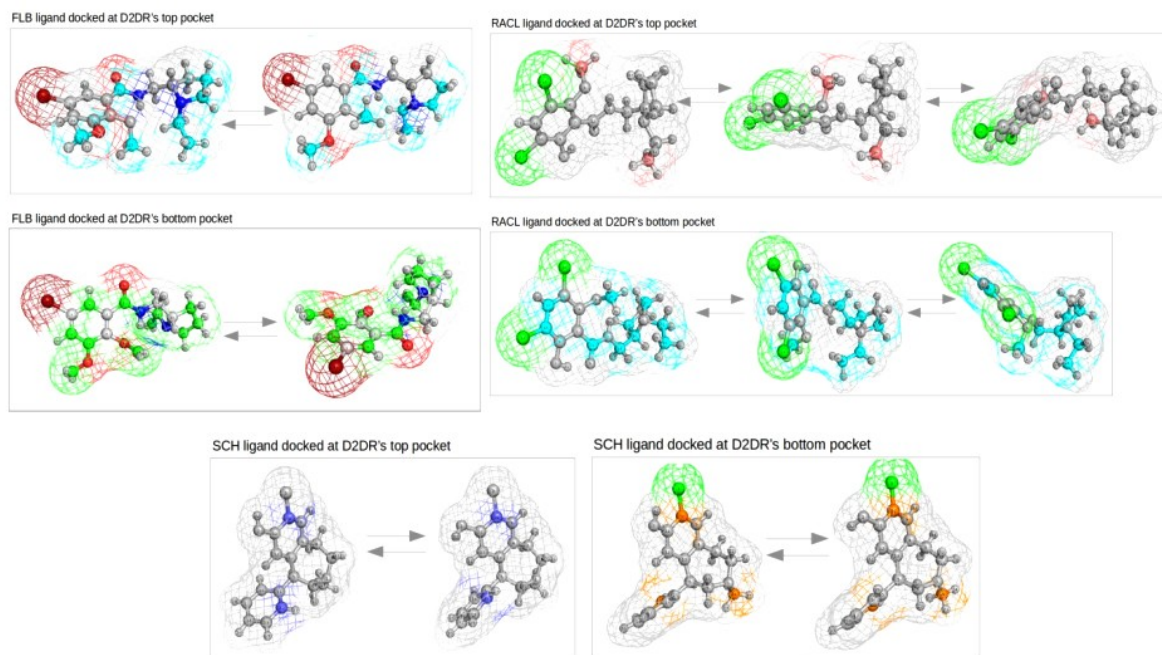


Figure 11. The most prominent motions for the three sets of ligands.

In good agreement with RMSD and gyration profiles, the SCH ligand showed lower flexibility rates. For the uptake of D2DR, only two C atoms and several peripheral H atoms were involved in the collective movements of the SCH ligand. Slightly larger fluctuations were observed for the SCH ligand docked at the bottom part of the receptor, where its main components involve C-Cl and -CH₃ peripheral rotational movements.

Although our docking results showed, as expected, significantly lower absolute values for ligands considered at the bottom part of the receptor, the total interaction energy values compared between the two sets of ligands (top and bottom) were almost comparable. Moreover, the SCH ligand situated at the bottom part of D2DR showed the highest total interaction energy value. The general behaviors for FLB and RACL ligands were similar at both D2DR positions, with few exceptions where the FLB ligand showed larger variations, such as SASA or RMSD average values.

Our interest in studying the SCH-23390 ligand was mainly related to the hypothesis that, even if it corresponds to the affinities of the D1 subunit, the compound could also have minimal effects on the D2 type of receptor [29, 30] and, according to the literature, there are no theoretical studies focused on D2DR complexes that interact with SCH.

2.4 Biophysical Insights on the Interaction Mechanism between Multiple Single Stranded DNAs: A1/A2@GNR and miR21, anti-miR21, miR21-sp, random APTs

In HD conditions, the aptamers' binding specificity to mutant/altered huntingtin structures activates targeted post-translational modifications at the polyglutamine tract's level and may serve as "huntingtin biosensors". Notably, these interactions occur for elongated polyQ tracts. As a result of the aptamers' binding, it has been shown that cellular ATP levels significantly increases, with a lower hyper-vulnerability to cellular stresses [31]. Therefore, transfected single-stranded DNA oligonucleotides may have protective environmental cellular effects by altering or even blocking further mutant huntingtin interactions [31].

The integration of ssDNAs in recognition models requires a detailed and controlled sequential and structural performance. The aptamers' dynamic (and hard to control) evolution might induce unsuited structural modifications by triggering "inadequate affinities" and a lower binding specificity. Within this framework (*Figure 12*), the following study emphasizes dynamical and structural changes for two types of interacting ssDNA systems: (1) a binary set consisting of A1-alone/A2-attached onto a AU surface with anti-sheet conformations.miR21, miR21, random, and miR21-sp as interacting partners and (2) four ternary systems where the aptamers (anti-miR21, miR21, random and miR21-sp) were considered in interaction with both A1 and A2 (attached onto the AU surface) strands. The DNA sequences for each aptamer are illustrated in *Figure 13*.

For the binary systems, the maximum gyration value of 4.43 nm was obtained for A2@GNRs in interaction with the *random* aptamer, while the minimum Rg value of 3.12 nm was correlated with the A1-anti(miR21). The aptamers related to the ternary systems showed much higher Rg values, indicating an increased degree of elongation. Also, the RMSD values were lower for A1 binary systems, compared to A2@GNRs systems. The maximum RMSF (average) value of 0.79 nm were obtained for the A1 interaction complex with the miR21-sp aptamer (*Figure 14*). Minimum atomic fluctuations with an average value of 0.66 nm were obtained for the random aptamer in interaction with A1.

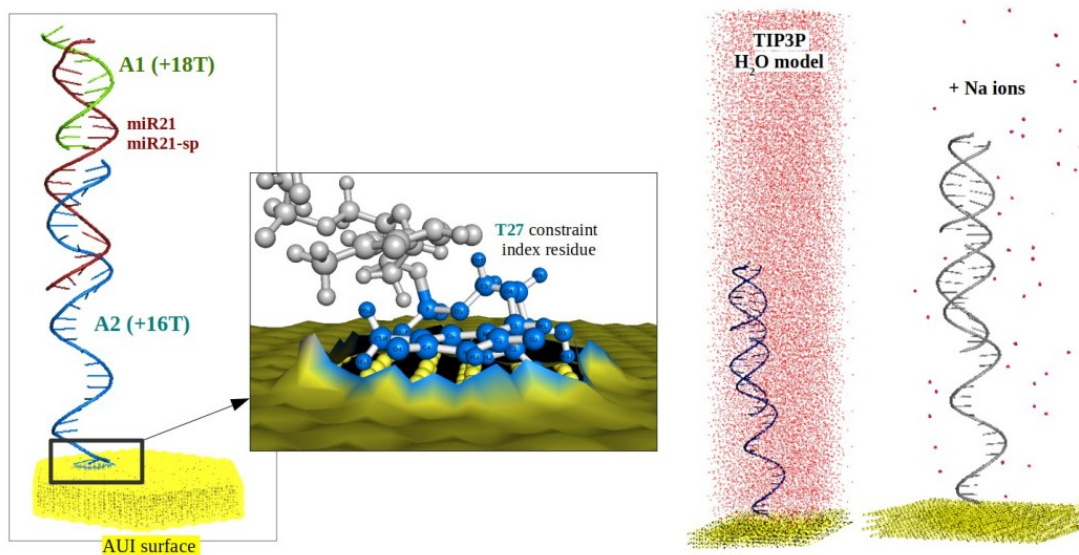


Figure 12. The input 3D representation of solvated and neutralized systems.

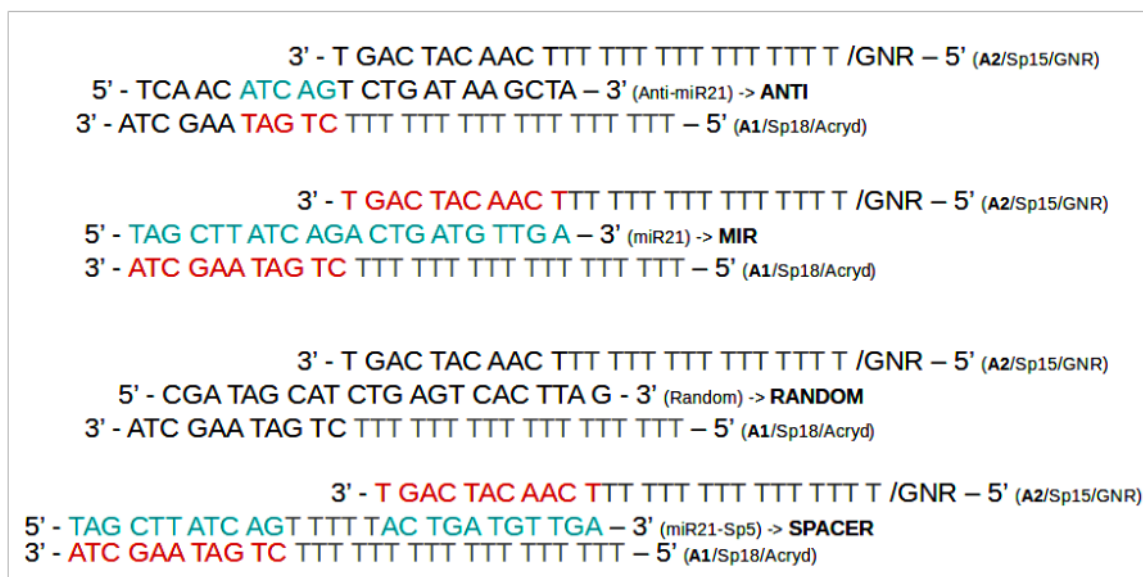


Figure 13. Single-stranded DNA input sequences.

For all A2@GNRs interaction systems, the RMSD values were comparable and showed a maximum value of 1.13 nm in interaction with the anti-miR21 aptamer, while a minimum RMSD value of 1.06 nm was obtained for interactions between A2@GNRs with miR21 aptamer. With respect to the ternary systems, the minimum value (of 1.35 nm) was noted for the miR21 sequence. Maximum RMSF values (of 1.58 nm and 1.53 nm) were observed for anti-miR21 and miR21-sp aptamers.

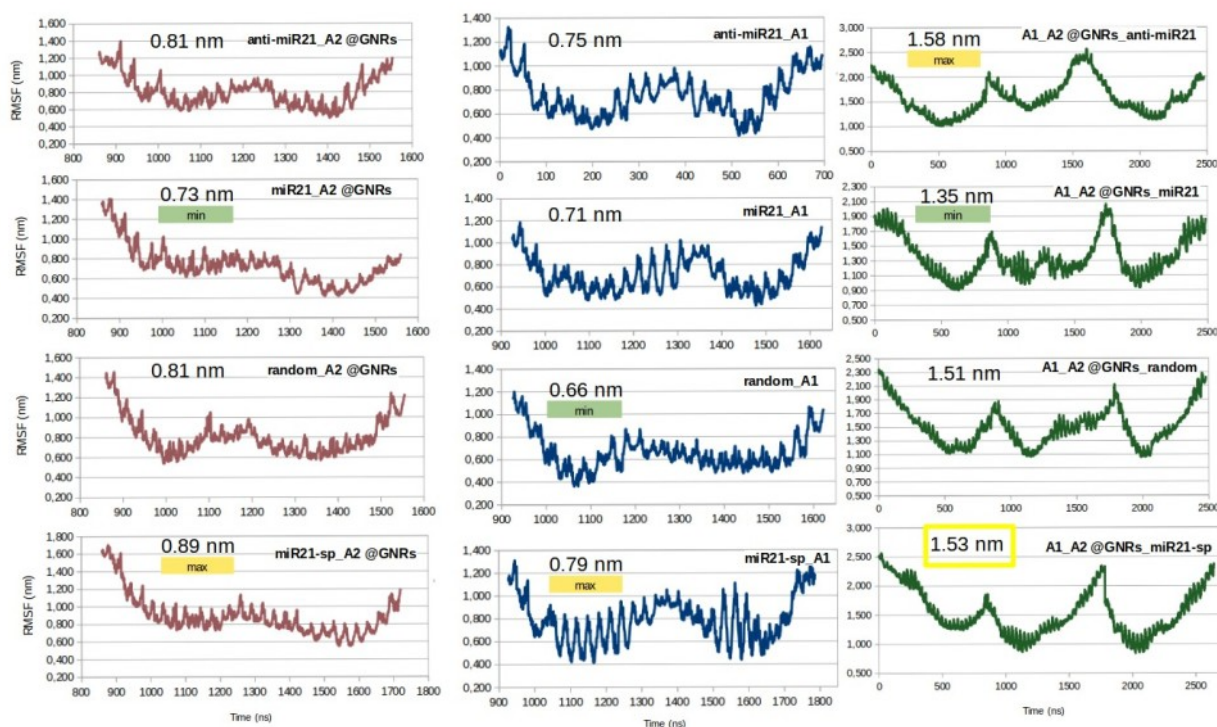


Figure 14. RMSF profiles for all interacting complexes.

In agreement with the previously discussed measurements, the maximum number of H bindings was obtained for the interaction systems between A1/A2 @ GNRs with the miR21-sp aptamer. The number of H bonds between A1 and miR21-sp (*Figure 15*) was about 30, while between A2@GNRs and miR21-sp, the H bonds formed reached a maximum number of 14. At the same time, an increased number of H bonds was also correlated to A1/A2@GNR systems in interaction with miR21 aptamer. The minimum number of H bonds was obtained for the interaction systems related to anti-miR21 and random aptamers.

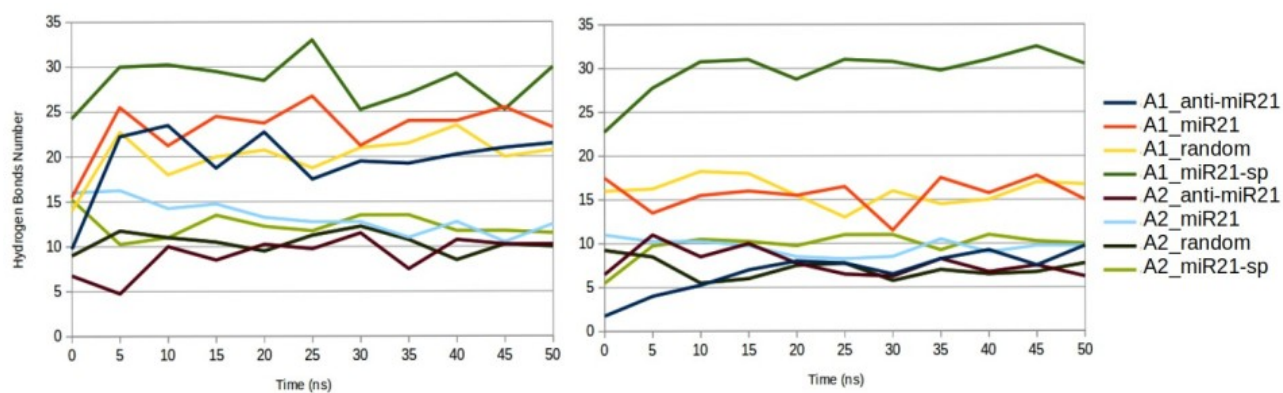


Figure 15. H-bond plots for A1/A2@GNRs and APTs interacting complexes.

For ternary systems, the weakest interactions were observed for the *random* aptamer. On the other hand, according to the calculated total energies, the strongest interactions were obtained for the miR21-sp and miR21 aptamers. The structural behavior observed in the case of miR21 and miR21-sp systems is strongly correlated to their maximum values of the gyration radius values, with the increased atomic fluctuations and the maximum number of H bonds.

The resulted trajectories (see *Figures 16, 17*) identify an increased affinity between DNA chains based on nucleotide's complementarity rules for the interacting systems with miR21 and miR21-sp aptamers. Furthermore, increased dynamic stabilities were observed for miR21-sp interacting complexes, due to the insertion of 5 thymine residues in the middle of the sequence.

The weakest interactions are correlated with a much lower number of H-bonds for the interacting complexes with random aptamer. Moreover, the principal component analysis revealed discontinuous fluctuation rates within the involved structures, therefore leading to higher RMSF profiles for both A1/A2@GNR binary systems. In the same manner, anti-miR21 aptamer showed similar dynamical profiles but with a slightly higher interaction energy pattern influenced by the presence of a few interacting complementary nucleotides.

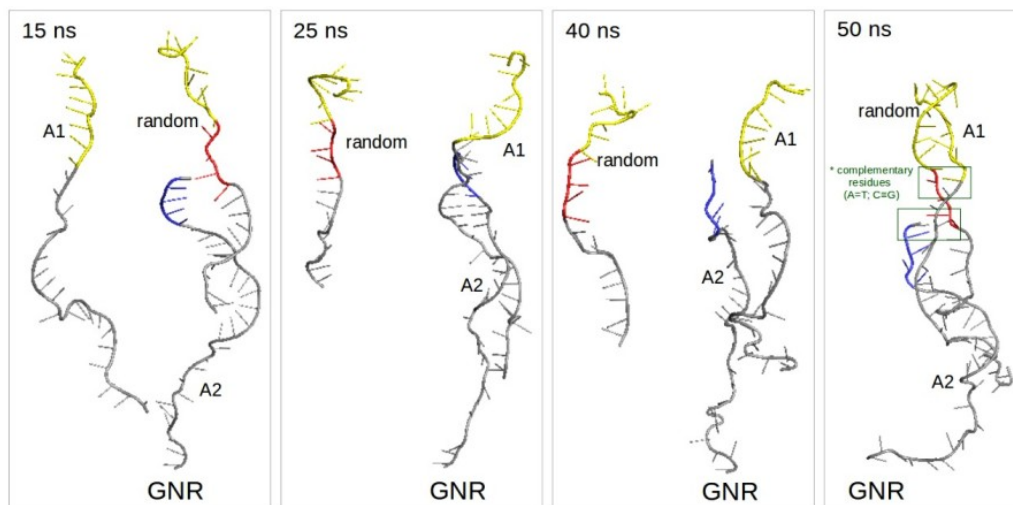


Figure 16. Resulted trajectories for the ternary interacting systems with *random* aptamer.

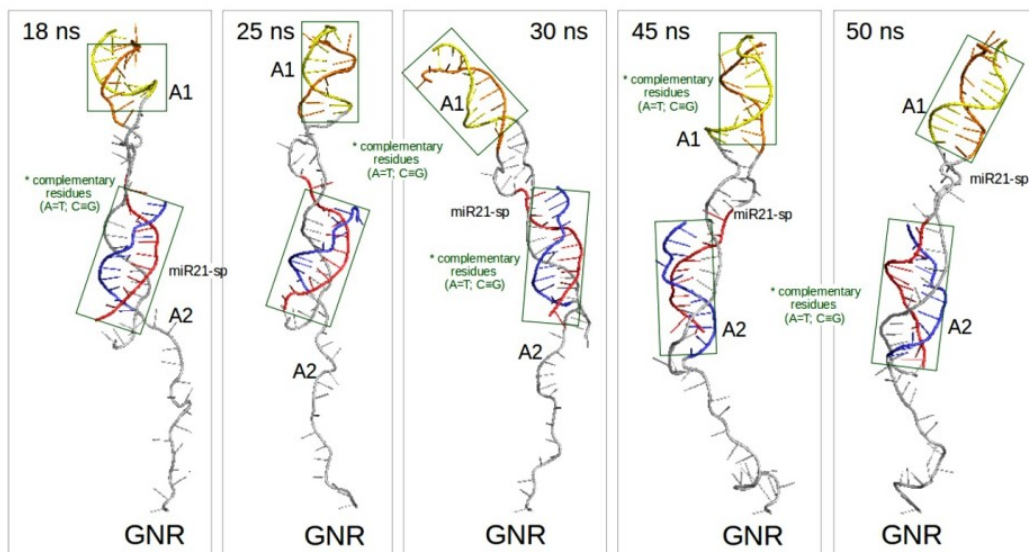


Figure 17. Resulted trajectories for the ternary interacting systems with *miR21-sp* aptamer.

The general conclusions, extracted from the presented theoretical studies, regarding each investigated aspect are:

1. Despite the relevant findings on HTT's structural behavior, the function and the polymerization process that describes how the mutation is formed still remains unknown. In general, it is strongly believed that as the Q-length increases the polyQ structures tend to adopt more β -sheet conformations. Moreover, the N17 domains are also able to form β -like structures as the Q-length increases. Another structural behavior that must be taken into account is that the increased number of Q residues in the polyQ tracts leads to condensed structures with highly compact distributed residues in the polyQ regions, therefore the shape of the m-HTT becomes more spherical as the number of the Q residues increases.

Although the random models of 4P, 7P, and 9P mutations did not suggest specific behavioral patterns, for the 9P(EM) model's helical content, the R_g results showed significant decreases in the averaged values, which were afterwards correlated with high RMS fluctuations and consequently to potential disruptions of the helical conformation. Furthermore, the results showed no β -sheet content in our trajectories, and consequently, our results are in agreement with the hypothesis that proline is able to break both α -helix and β -sheet contents.

Thus, we propose a quantitative mutational threshold of 9P residues with spots of mutation on the edges and in the middle of the helix for higher rates of helical disruption.

2. The highest compactness level of CaM interacting with the 9P(EM) involves drastic structural changes of the CaM's helical linker that might increase the chance for the CaM's lobes to overlap. The RMS fluctuation rates are higher for the 9P(EM) model, while the minimum distance values between the edges of the helix, for the same model, significantly decreased implying drastic structural transitions from α -helices to turns and highly soluble random coils. Considering these changes we can relate the structural behavior of our proposed model to its interaction energies that were much lower in comparison to the 45Qs-HTT mutant. Consequently, at a molecular level, the expanded polyQ tracts can increase their affinities to other mutant protein interactions.

3. The highest absolute value of the total interaction energy for the lower part of the D2DR was observed for the SCH ligand, while for the top part of D2DR, the highest interaction energy values were correlated to RACL ligand. Moreover, while the FLB ligand manifests a slight tendency to emerge out of the receptor's bottom pocket, the SCH and RACL ligands showed greater binding affinity for both receptor's pockets while remaining inside of D2DR.

Thus, according to our results the RACL ligand docked at the top pocket of D2DR is clearly the most efficient ligand for the modeled receptor-ligand interacting complex.

4. For the last study of interest, the total interaction energy values for A1-APTs binary systems are much higher when compared to A2@GNR-APTs. From a structural point of view, miR21 and miR21-sp aptamers exhibit similar structural patterns. Last but not least, the gyration profiles for A2@GNR showed an increased compactness level suggesting that the A2's tail (with 16 T residues) tends to bend onto the gold surface. Moreover, the binary A2@GNR/A1-miR21-sp complexes presented the highest number of H-bonds due to the spacer's increased length (27 nucleotides, including the 5T in the middle of it).

Therefore, we can consider the A2-miR21-sp (together with A1) and miR21 interacting complexes as the most suitable ones for further experimental investigations.

1. Genheden S., Reymer A., Saenz-Méndez P. and Eriksson L.A, (2017) Chapter 1: Computational Chemistry and Molecular Modelling Basics, in *Computational Tools for Chemical Biology*, 1-38.
2. Nair P. C, Miners J. O. (2014) Molecular dynamics simulations: from structure function relationships to drug discovery, In *Silico Pharmacol.*
3. Nair P. C, Miners J. O. (2014) Molecular dynamics simulations: from structure function relationships to drug discovery, In *Silico Pharmacol.*
4. Abraham M.J., van der Spoel D., Lindahl E., Hess B., and the GROMACS development team, *GROMACS User Manual version 2018.*
5. Reiner A., Dragatsis I., Dietrich P. (2011) Genetics and neuropathology of Huntington's disease. *Int Rev Neurobiol.* 98:325-372.
6. Kandel E. R, Schwartz J. H, Jessel T. M, eds. (2000) Ch. 9: Propagated signaling: the action potential. *Principles of Neural Science.* McGraw-Hill Professional.
7. Masino L., Kelly G., Leonard K., Trottier Y., and Pastore A. (2002) Solution structure of polyglutamine tracts in GST-polyglutamine fusion proteins. *FEBS Lett.* 513, 267–72.
8. Bennett M. J., Huey-Tubman K. E., Herr A. B., West A. P., Jr., Ross S. A., and Bjorkman P. J. (2002) A linear lattice model for polyglutamine in CAG-expansion diseases. *Proc. Natl. Acad. Sci. U. S. A.* 99, 11634–11639.
9. Kang H., Vázquez F. X., Zhang L., Das P., Toledo-Sherman L., Luan B., Levitt M., and Zhou R. (2017) Emerging β -sheet conformations in super-compact Huntingtin exon-1 mutant structures. *J. Am. Chem. Soc.* 139 (26), 8820–8827.
10. Marques Sousa C., and Humbert S. (2013) Huntingtin: here, there, everywhere! *J. Huntington's Dis.* 2, 395–403.
11. Saudou F., Finkbeiner S., Devys D., and Greenberg M. E. (1998) Huntingtin Acts in the Nucleus to Induce Apoptosis but Death Does Not Correlate with the Formation of Intranuclear Inclusions. *Cell* 95 (1), 55–66.
12. Jimenez-Sanchez M., Licitra F., Underwood B. R., and Rubinsztein D. C. (2017) Huntington's Disease: Mechanisms of Pathogenesis and Therapeutic Strategies. *Cold Spring Harbor Perspect. Med.* 7, No. a024240.
13. Priya B. S., and Gromiha M. M. (2019) Structural insights into the aggregation mechanism of huntingtin exon 1 protein fragment with different polyQ lengths. *J. Cell. Biochem.* 120, 10519–10529.

14. Nagai Y., Inui T., Popiel H. A., et al. (2007) A toxic monomeric conformer of the polyglutamine protein. *Nat. Struct. Mol. Biol.* 14 (4), 332–340.
15. Bhattacharyya A., Thakur A. K., Wetzel R., et al. (2006) Oligoproline effects on polyglutamine conformation and aggregation. *J. Mol. Biol.* 355, 524–535.
16. Altschuler E. L., Hud N. V., Mazrimas J. A., and Rupp B. (1997) Random coil conformation for extended polyglutamine stretches in aqueous soluble monomeric peptides. *J. Pept. Res.* 50, 73–75.
17. Kim M. (2013) Beta conformation of polyglutamine track revealed by a crystal structure of Huntingtin N-terminal region with insertion of three histidine residues. *Prion* 7 (3), 221–228.
18. Neveklavska M., Clabough E. B., Steffan J. S., and Zeitlin S. O. (2012) Deletion of the huntingtin proline-rich region does not significantly affect normal huntingtin function in mice. *J. Huntington's Dis.* 1 (1), 71–87.
19. Caron N. S., Desmond C. R., Xia J., and Truant R. (2013) Polyglutamine domain flexibility mediates the proximity between flanking sequences in huntingtin. *Proc. Natl. Acad. Sci. U. S. A.* 110 (36), 14610–14615.
20. Długosz M., and Trylska J. (2011) Secondary structures of native and pathogenic huntingtin N terminal fragments. *J. Phys. Chem. B* 115 (40), 11597–11608.
21. Ogawa H., Nakano M., Watanabe H., Starikov E. B., Rothstein S. M., and Tanaka S. (2008) Molecular dynamics simulation study on the structural stabilities of polyglutamine peptides. *Comput. Biol. Chem.* 32 (2), 102–110.
22. Chen S., Berthelie V., Yang W., and Wetzel R. (2001) Polyglutamine aggregation behavior in vitro supports a recruitment mechanism of cytotoxicity. *J. Mol. Biol.* 311, 173–82.
23. Kelley N. W., Huang X., Tam S., Spiess C., Frydman J., and Pande V. S. (2009) The predicted structure of the headpiece of the huntingtin protein and its implications on huntingtin aggregation. *J. Mol. Biol.* 388 (5), 919–927.
24. Wang Y., and Voth G. A. (2010) Molecular Dynamics Simulations of Polyglutamine Aggregation Using Solvent-Free Multiscale Coarse-Grained Models. *J. Phys. Chem. B* 114, 8735.
25. Adegbuyiro A., Sedighi F., Pilkington A. W., Groover S., and Legleiter J. (2017) Proteins containing expanded polyglutamine tracts and neurodegenerative disease. *Biochemistry* 56 (9), 1199–1217.

26. Lakhani V. V., Ding F., and Dokholyan N. V. (2010) Polyglutamine Induced Misfolding of Huntingtin Exon1 is Modulated by the Flanking Sequences. *PLoS Comput. Biol.* 6 (4), No. e1000772.
27. **Moldovean S. N. and Chiş V. (2020) Specific Key-Point Mutations along the Helical Conformation of Huntingtin-Exon 1 Protein Might Have an Antagonistic Effect on the Toxic Helical Content's Formation. *ACS Chemical Neuroscience*, 11, 2881-2889.**
28. **Moldovean S. N. and Chiş V. (2021) Decreased Interactions between Calmodulin and a Mutant Huntingtin Model Might Reduce the Cytotoxic Level of Intracellular Ca²⁺ : A Molecular Dynamics Study. *International Journal of Molecular Sciences*. 22(16):9025.**
29. Breese G. R, Mueller R. A. (1985) SCH-23390 antagonism of a D2 dopamine agonist depends upon catecholaminergic neurons. *Eur J Pharmacol.* 113(1):109-114.
30. Derlet R. W, Albertson T. E, Rice P. (1990) The Effect of SCH 23390 Against Toxic Doses of Cocaine, Amphetamine and Methamphetamine. *Life Sciences.* 47 (9): 821–827.
31. Shin B., Jung R., Oh H., Owens G. E., Lee H., Kwak S., Lee R., Cotman S. L., Lee J. M., MacDonald M. E., Song J. J., Vijayvargia R., Seong I. S. (2018) Novel DNA Aptamers that Bind to Mutant Huntingtin and Modify Its Activity. *Mol Ther Nucleic Acids.*, 11:416-428.

List of publications related to this thesis

1. **Moldovean S. N.** and Chiş V. (2020) Molecular Dynamics Simulations Applied to Structural and Dynamical Transitions of the Huntingtin Protein: A Review. ACS Chemical Neuroscience,11(2), 105-120. IF = 4.418 AIS = 1.07
2. **Moldovean S. N.** and Chiş V. (2020) Specific Key-Point Mutations along the Helical Conformation of Huntingtin-Exon 1 Protein Might Have an Antagonistic Effect on the Toxic Helical Content's Formation. ACS Chemical Neuroscience, 11, 2881-2889. IF = 4.418 AIS = 1.07
3. **Moldovean S. N.** and Chiş V. (2021) Decreased Interactions between Calmodulin and a Mutant Huntingtin Model Might Reduce the Cytotoxic Levels of Intracellular Ca²⁺ : A Molecular Dynamics Study. International Journal of Molecular Sciences, 22(16):9025. IF =5.923 AIS = 1.123
4. **Moldovean S. N.**, Timaru D-G. and Chiş V. All-atom Molecular Dynamics Investigations on the Interactions between D2-subunit Dopamine Receptor and Three 11 C-labeled Radiopharmaceutical Ligands, *submitted, under review*.
5. Gliga L-E., Iacob B-C., **Moldovean S. N.**, Spivak D. A., Bodoki E., and Oprean R. Affinity capillary electrophoretic study of the molecular interactions between DNA aptamers for the development of biomarker platforms for microRNA detection, *submitted, under review*.

Oral presentations at national and international conferences:

1. **Moldovean S. N.** Structural Insights into m-HTT Protein, The National Conference of doctoral students from “Universitaria” Consortium 2019, Bucharest, 26-27 September 2019.
2. **Moldovean S. N.** Huntington’s Disease in Molecular Dynamics, The National Conference of Medical Physics 2020, November 7 2020.
3. **Moldovean S. N.** Specific key-point mutations along the helical conformation of Huntingtin-Exon1 protein might have an antagonistic effect on the toxic helical content’s formation, International Conference on Interactive Molecular Dynamics and Applications 2021, Amsterdam, 8-9 February 2021 (*Best presentation award*).